Hydrodynamic friction of fakir-like superhydrophobic surfaces

ANTHONY M. J. DAVIS AND ERIC LAUGA†

Department of Mechanical and Aerospace Engineering, University of California San Diego,
9500 Gilman Drive, La Jolla, CA 92093-0411, USA

A fluid droplet located on a superhydrophobic surface makes contact with the surface only at small isolated regions, and is mostly in contact with the surrounding air. As a result, a fluid in motion near such a surface experiences very low friction, and superhydrophobic surfaces display strong drag reduction in the laminar regime. Here we consider theoretically a superhydrophobic surface composed of circular posts (so-called fakir geometry) located on a planar rectangular lattice. Using a superposition of point forces with suitably spatially dependent strength, we derive the effective surface-slip length for a planar shear flow on such a fakir-like surface as the solution to an infinite series of linear equations. In the asymptotic limit of small surface coverage by the posts, the series can be interpreted as Riemann sums, and the slip length can be obtained analytically. For posts on a square lattice, our analytical prediction of the dimensionless slip length, in the low surface coverage limit, is in excellent quantitative agreement with previous numerical computations.

---

1. Introduction

When a small droplet of liquid is deposited on a hydrophobic surface whose geometry is sufficiently rough, in certain situations the liquid will not fill the roughness grooves but will instead adopt a lower-energy configuration, sometimes called a fakir state, where it remains on top of the surface topography (figure 1*a*). Exemplified by the Lotus leaf, surfaces for which this situation occurs are referred to as superhydrophobic (or more generally, super-repellent), and their geometrical and physical description has been the subject of several recent studies (Onda *et al.* 1996; Bico, Marzolin & Quéré 1999; Feng *et al.* 2002; de Gennes F. Brochard-Wyart & Quéré 2004; Quéré 2008; Roach, Shirtcliffe & Newton 2008).

One of the remarkable properties of superhydrophobic surfaces is their low friction opposing the flow (Rothstein 2010). Since the fluid next to such a surface makes contact with the solid at only a few isolated points and is mostly in contact with air, the shear stresses opposing fluid motion are small, and fluids in fakir states can move very easily. In these situations, the surface friction is usually quantified by a slip length, λ, which is the fictitious distance below the surface where the no-slip condition would be valid on average (Neto *et al.* 2005; Bocquet & Barrat 2007;

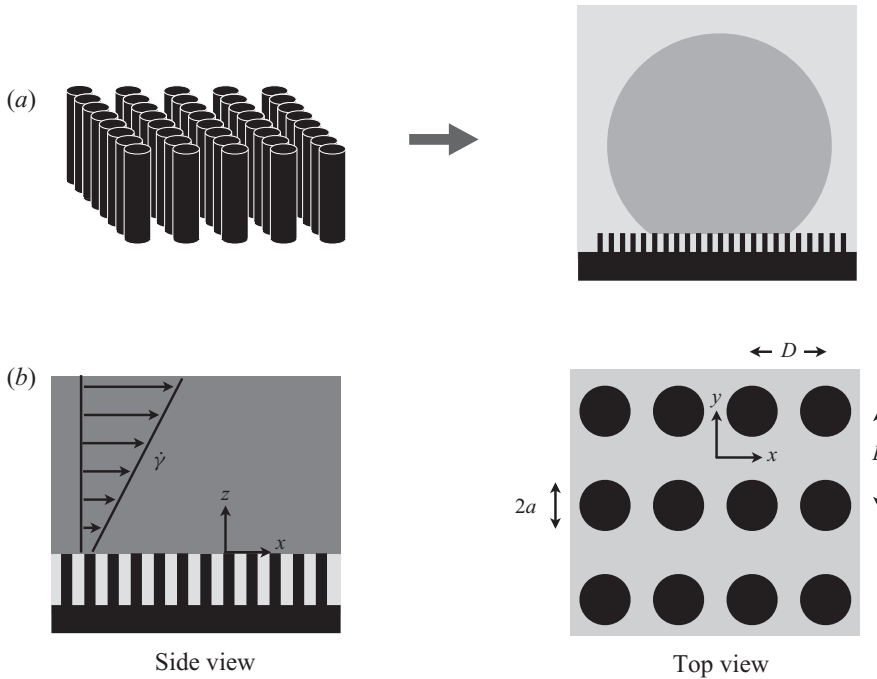† Email address for correspondence: elauga@ucsd.edu

FIGURE 1. Fakir-like superhydrophobic surfaces and set-up for our calculation. (*a*) A droplet deposited on surface composed of tall hydrophobic posts can remain in a fakir superhydrophobic state where it partially sits on the posts and partially on the air. (*b*) Definition sketches. A viscous fluid of shear viscosity μ sits in a fakir state on a two-dimensional array of circular posts. The posts have radius a, and are arranged on a rectangular lattice of periodicity D and L along the x- and y-directions, respectively. A shear flow with shear rate $\dot{\gamma}$ is imposed in the fluid along the x-direction, and perpendicularly to the surface. In-between the posts, the fluid–air interface is assumed to remain flat and parallel to the superhydrophobic surface.

Lauga, Brenner & Stone 2007); no-slip corresponds to $\lambda = 0$, while superhydrophobic surfaces with $\lambda > 0$ have a lower effective friction than no-slip.

From a practical standpoint, many different methods exist to design and produce superhydrophobic surfaces (Feng *et al.* 2002; Roach *et al.* 2008), and they lead to surfaces with either random or controlled geometrical features. Surfaces with random topography are known to show slip (Gogte *et al.* 2005; Choi & Kim 2006; Joseph *et al.* 2006). Planar surfaces with controlled geometry are of two types. The first type of surface is associated with one-dimensional features such as long grooves, usually aligned parallel or perpendicular to the flow direction, and for which a lot of experimental (Ou, Perot & Rothstein 2004; Ou & Rothstein 2005; Choi *et al.* 2006; Truesdell *et al.* 2006; Maynes *et al.* 2007; Tsai *et al.* 2009) and modelling (Lauga & Stone 2003; Cottin-Bizonne *et al.* 2004; Davies *et al.* 2006; Maynes *et al.* 2007; Ng & Wang 2009; Teo & Khoo 2009) work has characterized their frictional properties.

The second type of surface is associated with two-dimensional patterning, usually a series of vertical posts distributed on a regular lattice, as illustrated schematically in figure 1(*a*). Only a handful of studies have focused on the friction of this type of surface, either experimentally (Lee, Choi & Kim 2008) or theoretically (Ybert *et al.* 2007; Ng & Wang 2010). In the limit of low solid fraction, these two-dimensional

surfaces are expected, however, to display much lower friction (algebraic divergence of the slip length) than one-dimensional surfaces (logarithmic divergence) (Ybert *et al.* 2007), and it is thus important to be able to accurately predict their friction properties. This is the goal of the present paper.

Previous theoretical work focusing on surfaces composed of posts on a lattice, found that if $\phi_s < 1$ denotes the areal density of the horizontal cross-section of the posts, the effective slip length of the superhydrophobic surface, non-dimensionalized by the typical distance, L, between the posts, behaves in the limit of low ϕ_s as

$$\frac{\lambda}{L} \sim \frac{A}{\sqrt{\phi_s}} - B \tag{1.1}$$

(Ybert *et al.* 2007; Ng & Wang 2010). In (1.1), the positive coefficients, A and B, depend on the lattice and posts geometry but not ϕ_s, and can be fitted to numerical computations, while the square-root scaling can be physically rationalized as follows. The shear stress acting on the posts scales as $\tau \sim \phi_s \mu \dot{\gamma}_s$, where μ is the fluid viscosity and γ_s is the typical shear rate around a post. If U is the typical fluid velocity between the posts, and a is the typical post radius, we have $\dot{\gamma}_s \sim U/a$, and since $\lambda \sim \mu U/\tau$ we obtain $\lambda \sim a/\phi_s$. As the solid fraction scales as $\phi_s \sim (a/L)^2$, we have $a \sim L\phi_s^{1/2}$, and hence we obtain the square-root scaling of (1.1), namely $\lambda/L \sim 1/\phi_s^{1/2}$ (Ybert *et al.* 2007).

In this study, we consider the simplest possible geometry for flow over a fakir-like superhydrophobic surface, namely vertical posts with circular cross-section located on a regular rectangular lattice, and we provide two results. Firstly, we present an analytical method based on a linear superposition of flow singularities to accurately determine the friction (i.e. the effective surface-slip length) for all surface coverage. Secondly, by asymptotically considering the case of low solid fraction, ϕ_s, we mathematically derive the scaling coefficients A and B governing (1.1), thereby predicting analytically the effective surface-slip length. Our results are compared to previous computational work, and show excellent agreement.

2. Calculation of the effective surface-slip length

2.1. *Problem outline*

Our geometry is illustrated in figure 1(*b*). A viscous fluid of viscosity μ is located in a fakir state on a two-dimensional array of circular posts. The posts have radius a, and are arranged on a rectangular lattice of periodicity D and L along the x- and y-directions, respectively, with $2a < \min(D, L)$. A shear flow with shear rate $\dot{\gamma}$ is imposed in the far field by the prescribed velocity along the x-direction, with shear perpendicularly to the surface along the z-direction. The prescribed velocity is thus given by

$$\boldsymbol{v} \sim (\dot{\gamma}z + U)\boldsymbol{e}_x \quad \text{as} \quad z \to \infty, \tag{2.1}$$

where $\boldsymbol{e}_x$, $\boldsymbol{e}_y$, $\boldsymbol{e}_z$ denote unit vectors parallel to the axes, and thus U denotes the effective slip velocity at the fakir contact plane, $z = 0$. In-between the posts, the fluid–air interface is assumed to remain flat and parallel to the underlying superhydrophobic surface with no shear acting on it. The flow satisfies the no-slip boundary condition on the top of the circular posts.

Our aim is to accurately estimate the effective slip length, that is, the mean speed/mean shear ratio at the superhydrophobic plane. As in our recent calculation for a moving grid (Davis & Lauga 2009), here the basic tool is the Stokes flow

generated by a similarly periodic array of aligned, parallel point forces directed in their plane. In addition, the force-density function is assumed, for the leading approximation, to have an inverse square root rim singularity, as in the creeping flow past a disk. The resulting linear system has matrix elements that are interpreted as Riemann sums and the limit double integrals are easily evaluated. The dominant error arises from the missing term in the double sum and thus precise estimates can be obtained for the two coefficients in (1.1).

2.2. *Calculation using a superposition of singularities*

The Reynolds number of the viscous incompressible flow is assumed to be sufficiently small for the velocity field v to satisfy the creeping flow (Stokes) equations (Happel & Brenner 1965)

$$\mu \nabla^2 v = \nabla p, \qquad \nabla \cdot v = 0, \tag{2.2}$$

where p is the dynamic pressure. The fluid motion can be represented as due to a distribution of tangentially directed Stokeslets over the circular regions, augmented by the uniform flow $U e_x$. The density functions must be both periodic in two dimensions and symmetric with respect to the sides of each rectangle. The field due to a two-dimensional rectangular array, periods D and L, of point forces of strength $4\pi\mu U \sqrt{DL}$ directed parallel to the flow at infinity, is governed by

$$\nabla \cdot v_A = 0, \tag{2.3}$$

$$\left.\begin{aligned}
\mu \nabla^2 v_A - \nabla p_A &= 4\pi\mu U \sqrt{DL} e_x \delta(z) \sum_{n_1=-\infty}^{\infty} \sum_{n_2=-\infty}^{\infty} \delta(x - n_1 D)\delta(y - n_2 L), \\
&= \frac{4\pi\mu U}{\sqrt{DL}} e_x \delta(z) \sum_{m_1=-\infty}^{\infty} \sum_{m_2=-\infty}^{\infty} \exp\left[2\pi i \left(\frac{m_1 x}{D} + \frac{m_2 y}{L}\right)\right].
\end{aligned}\right\} \tag{2.4}$$

The $m_1 = 0 = m_2$ term in (2.4) yields the anticipated shear at infinity and, as in Davis & Lauga (2009), the flow generated by the oscillatory forcing is readily found by Fourier transform techniques (Hasimoto 1959). Thus the flow governed by (2.4) is compactly expressed as

$$v_A = U \left[\left(\frac{2\pi z}{\sqrt{DL}} - S_1\right) e_x + \nabla \frac{\partial S_2}{\partial x}\right], \quad p_A = \mu U \frac{\partial S_1}{\partial x}, \tag{2.5}$$

where, with a prime denoting that the $m_1 = 0 = m_2$ term is missing,

$$S_1 = \frac{1}{\sqrt{DL}} \sum_{m_1} \sum_{m_2}' \frac{1}{\sqrt{(m_1/D)^2 + (m_2/L)^2}}$$
$$\times \exp\left[2\pi\left(\frac{im_1 x}{D} + \frac{im_2 y}{L} - z\sqrt{\left(\frac{m_1}{D}\right)^2 + \left(\frac{m_2}{L}\right)^2}\right)\right] \tag{2.6}$$

and

$$S_2 = -\frac{1}{8\pi^2\sqrt{DL}} \sum_{m_1} \sum_{m_2}' \frac{1}{(m_1/D)^2 + (m_2/L)^2}\left(\frac{1}{\sqrt{(m_1/D)^2 + (m_2/L)^2}} + 2\pi z\right)$$
$$\times \exp\left[2\pi\left(\frac{im_1 x}{D} + \frac{im_2 y}{L} - z\sqrt{(m_1/D)^2 + (m_2/L)^2}\right)\right], \tag{2.7}$$

with $S_1 = \nabla^2 S_2$. Only the velocities at the posts and at infinity are needed for the subsequent analysis. The solution (2.5) shows that

$$\boldsymbol{v}_A \sim \frac{2\pi U z}{\sqrt{DL}} \boldsymbol{e}_x \quad \text{as} \quad z \to \infty, \tag{2.8}$$

as well as

$$[\boldsymbol{v}_A]_{z=0} = U\boldsymbol{e}_x \left(-S_1 + \frac{\partial^2 S_2}{\partial x^2} \right)_{z=0}$$

$$= -\frac{U}{\sqrt{DL}} \boldsymbol{e}_x \sum_{m_1} \sum_{m_2}' \frac{C(m_1, m_2)}{\sqrt{(m_1/D)^2 + (m_2/L)^2}} \exp\left[2\pi i \left(\frac{m_1 x}{D} + \frac{m_2 y}{L} \right) \right], \tag{2.9}$$

where, after substitution of (2.6) and (2.7),

$$C(m_1, m_2) = 1 - \tfrac{1}{2} \frac{(m_1/D)^2}{(m_1/D)^2 + (m_2/L)^2}. \tag{2.10}$$

With suitably scaled force-density functions in the circular regions, the total flow field is given by

$$\boldsymbol{v} = U\boldsymbol{e}_x + \int_{-\pi}^{\pi} \int_0^a \left[\sum_{n=0}^{\infty} \frac{f_n(\alpha)}{\pi a^2} \cos 2n\beta \right]$$

$$\times \boldsymbol{v}_A[r\cos\theta - \alpha\cos\beta, r\sin\theta - \alpha\sin\beta, z]\alpha \, d\alpha \, d\beta, \tag{2.11}$$

in which the symmetry conditions restrict the density function to even cosines. The flow at infinity is determined by substituting (2.8) into (2.11), which gives

$$\boldsymbol{v} \sim U\boldsymbol{e}_x + \frac{2Uz}{a^2\sqrt{DL}} \boldsymbol{e}_x \int_{-\pi}^{\pi} \int_0^a \left[\sum_{n=0}^{\infty} f_n(\alpha) \cos 2n\beta \right] \alpha \, d\alpha \, d\beta, \quad \text{as} \quad z \to \infty. \tag{2.12}$$

Comparison with (2.1) then shows that the shear rate is given by

$$\dot{\gamma} = \frac{4\pi U}{a^2\sqrt{DL}} \int_0^a f_0(\alpha)\alpha \, d\alpha. \tag{2.13}$$

Thus only the mean force density contributes to the required slip length, λ, given by

$$\lambda = \frac{\text{slip speed}}{\text{shear rate}} = \frac{U}{\dot{\gamma}} = \frac{\sqrt{DL}}{4\pi} \frac{a^2}{\displaystyle\int_0^a f_0(\alpha)\alpha \, d\alpha}. \tag{2.14}$$

No-slip on the surface of the posts is achieved by enforcing $\boldsymbol{v} = 0$ at $z = 0$, $r < a$. The substitution of (2.9) into (2.11) gives the condition

$$1 = \frac{1}{\pi a^2 \sqrt{DL}} \int_{-\pi}^{\pi} \int_0^a \left[\sum_{n=0}^{\infty} f_n(\alpha) \cos 2n\beta \right] \sum_{m_1} \sum_{m_2}' \frac{C(m_1, m_2)}{M}$$

$$\times \exp[2\pi i M\{r\cos(\theta - \psi) - \alpha\sin(\theta - \psi)\}]\alpha \, d\alpha \, d\beta \quad (0 \leqslant r < a, -\pi < \theta \leqslant \pi), \tag{2.15}$$

where we have defined

$$M(\cos\psi, \sin\psi) = \left(\frac{m_1}{D}, \frac{m_2}{L} \right). \tag{2.16}$$

We next make two uses of the integral

$$\frac{1}{\pi} \int_{-\pi}^{\pi} \cos 2n\beta \exp[\pm 2\pi \mathrm{i} M\alpha \cos(\beta - \psi)] \, \mathrm{d}\beta = 2(-1)^n J_{2n}(2\pi M\alpha) \cos 2n\psi, \qquad (2.17)$$

where J_p refers to the Bessel function of the first kind of order p, first for a direct evaluation in (2.15) which gives,

$$1 = \frac{2}{a^2\sqrt{DL}} \int_0^a \sum_{n=0}^{\infty} f_n(\alpha)(-1)^n {\sum_{m_1}\sum_{m_2}}' \frac{C(m_1, m_2)}{M} J_{2n}(2\pi M\alpha)$$
$$\times \exp[2\pi \mathrm{i} Mr \cos(\theta - \psi)] \cos 2n\psi\,\alpha \, \mathrm{d}\alpha \quad (0 \leqslant r < a, -\pi < \theta \leqslant \pi), \quad (2.18)$$

and then to write down the Fourier coefficients in (2.18). Thus we obtain

$$\delta_{k0} = \frac{2}{a^2\sqrt{DL}} \int_0^a \sum_{n=0}^{\infty} f_n(\alpha)(-1)^{n-k} {\sum_{m_1}\sum_{m_2}}' \frac{C(m_1, m_2)}{M} J_{2n}(2\pi M\alpha)$$
$$\times J_{2k}(2\pi Mr) \cos 2k\psi \cos 2n\psi \, \alpha \, \mathrm{d}\alpha \quad (0 \leqslant r < a, k \geqslant 0), \quad (2.19)$$

where δ_{kn} denotes the Kronecker delta.

We next make two uses of the integral

$$\int_0^1 \frac{x^{2n+1} J_{2n}(bx)}{\sqrt{1-x^2}} \, \mathrm{d}x = \sqrt{\frac{\pi}{2b}} J_{2n+1/2}(b) \quad (n \geqslant 0, b > 0), \qquad (2.20)$$

first by introducing the conveniently scaled, inverse square root approximations for the force-density functions,

$$f_n(\alpha) \sim \frac{\alpha^{2n} c_n}{a^{2n-1}\sqrt{a^2 - \alpha^2}} \quad (n \geqslant 0), \qquad (2.21)$$

whose substitution in (2.19) yields

$$\delta_{k0} = \frac{1}{\sqrt{DL}} \sum_{n=0}^{\infty} c_n(-1)^{n-k} {\sum_{m_1}\sum_{m_2}}' \frac{C(m_1, m_2)}{M\sqrt{Ma}} J_{2n+1/2}(2\pi Ma)$$
$$\times J_{2k}(2\pi Mr) \cos 2k\psi \cos 2n\psi \quad (0 \leqslant r < a, k \geqslant 0). \quad (2.22)$$

Then the immaterial r-dependence can be jettisoned by applying the operator,

$$\int_0^a \left(\frac{r}{a}\right)^{2k+1} \frac{\mathrm{d}r}{\sqrt{a^2 - r^2}}, \qquad (2.23)$$

to (2.22), in order to obtain

$$\delta_{k0} = \frac{1}{2a\sqrt{DL}} \sum_{n=0}^{\infty} c_n(-1)^{n-k} {\sum_{m_1}\sum_{m_2}}' \frac{C(m_1, m_2)}{M^2} J_{2n+1/2}(2\pi Ma)$$
$$\times J_{2k+1/2}(2\pi Ma) \cos 2k\psi \cos 2n\psi \quad (k \geqslant 0). \quad (2.24)$$

Equation (2.24) is a symmetric infinite system of linear equations for the coefficients $\{c_n; n \geqslant 0\}$. The substitution of (2.21) into (2.14) then leads to the slip length as

$$\lambda = \frac{\sqrt{DL}}{4\pi c_0}. \qquad (2.25)$$

2.3. Asymptotic estimate of λ in the low-ϕ_s limit

An asymptotic estimate of the coefficients $\{c_n; n \geqslant 0\}$ is found by noting that

$$\frac{a^2}{DL} \sum_{m_1} \sum_{m_2} {}' \frac{C(m_1, m_2)}{(Ma)^2} J_{2n+1/2}(2\pi Ma) J_{2k+1/2}(2\pi Ma) \cos 2k\psi \cos 2n\psi, \qquad (2.26)$$

with

$$C(m_1, m_2) = 1 - \tfrac{1}{2} \cos^2 \psi, \quad Ma = \sqrt{\left(\frac{m_1 a}{D}\right)^2 + \left(\frac{m_2 a}{L}\right)^2}, \qquad (2.27)$$

is a Riemann sum, with increments $(a/D, a/L)$ in (x, y). In terms of polar coordinates (r, ψ), the integral has the separable form

$$\int_{-\pi}^{\pi} \int_0^{\infty} \left(1 - \tfrac{1}{2} \cos^2 \psi\right) J_{2n+1/2}(2\pi r) J_{2k+1/2}(2\pi r) \cos 2k\psi \cos 2n\psi \, \frac{\mathrm{d}r}{r} \, \mathrm{d}\psi = \frac{3\pi \delta_{nk}}{2\epsilon_n (4n+1)}, \qquad (2.28)$$

where we have used Neumann's symbol, $\epsilon_0 = 1$, $\epsilon_n = 2 \, (n > 0)$. The corresponding solution of (2.24) is

$$c_0 = \frac{4a}{3\pi\sqrt{DL}}, \quad c_n = 0 \, (n > 0), \qquad (2.29)$$

whose substitution into (2.14) yields the dimensionless slip coefficient,

$$\frac{\lambda}{\sqrt{DL}} \sim \frac{3\sqrt{DL}}{16a} = \frac{3}{16} \sqrt{\frac{\pi}{\phi_s}}, \qquad (2.30)$$

where $\phi_s = \pi a^2/DL$ is the fractional surface area covered by the circular regions. We note that this leading order term is symmetric in (D, L), the respective periods along and across the imposed shear flow, corresponding, therefore, to an isotropic surface friction at this order.

The leading error in the estimate (2.30) is due to the absence of a term associated with $m_1 = 0 = m_2$ in the Riemann sum. If the latter is regarded as having central function values, then the integrable singularity at the origin can be handled by exact integration over the rectangle centred at $(0, 0)$, assisted by small argument estimates of the Bessel functions. Then (2.28) has the additional term

$$-\frac{4\pi^{2n+2k+1}}{\Gamma(2n+3/2)\Gamma(2k+3/2)} \int_0^{a/2L} \int_0^{a/2D} \left[1 - \frac{x^2}{2(x^2+y^2)}\right] (x^2 + y^2)^{n+k-1/2} \, \mathrm{d}x \, \mathrm{d}y$$

$$= O\left[\left(\frac{a^2}{DL}\right)^{n+k+1/2}\right], \quad (2.31)$$

which is negligible unless $n = k = 0$. Evaluation for this case shows that (2.30) has the more accurate form,

$$\frac{\lambda}{\sqrt{DL}} \sim \frac{3}{16} \sqrt{\frac{\pi}{\phi_s}} - \frac{1}{\pi} \left[\sqrt{\frac{L}{D}} \ln\left(\frac{D}{L} + \sqrt{1 + \frac{D^2}{L^2}}\right) + \frac{1}{2}\sqrt{\frac{D}{L}} \ln\left(\frac{L}{D} + \sqrt{1 + \frac{L^2}{D^2}}\right)\right]. \qquad (2.32)$$

As a difference with the leading order term, the next-order term in (2.32) is not symmetric in (D, L), and therefore, rectangular lattices display anisotropic friction. Also note that this next-order term does not depend on the post radius a (and,
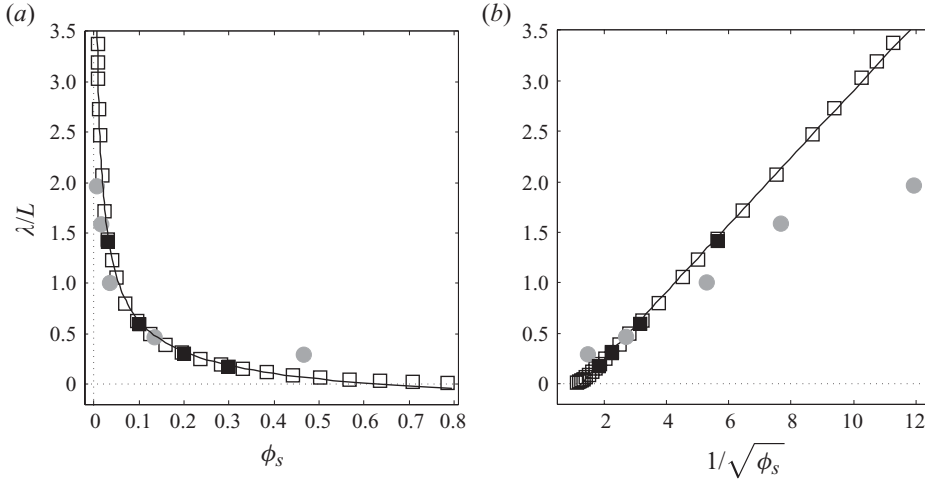
FIGURE 2. Results of our model, and comparison with previous computational and experimental work, in the case of a square lattice. Effective slip length, λ/L, as a function of the solid surface fraction, ϕ_s (a), and as a function of $1/\sqrt{\phi_s}$ (b). Solid line: simple asymptotic low ϕ_s model (2.33), empty squares: computations by Ng & Wang (2010), filled squares: computations by Ybert *et al.* (2007) and filled circles: experimental results by Lee *et al.* (2008).

therefore, ϕ_s). For a square array ($L = D$), (2.32) simplifies to

$$\frac{\lambda}{L} \sim \frac{3}{16}\sqrt{\frac{\pi}{\phi_s}} - \frac{3}{2\pi}\ln(1+\sqrt{2}), \qquad (2.33)$$

in the limit of low ϕ_s.

3. Results and comparison with previous work

We now compare the results of our asymptotic model to previous work considering circular posts organized on a square array. The comparison is displayed in figure 2, where we show the effective slip length, λ/L, as a function of the solid surface fraction, ϕ_s (a) and as a function of $1/\sqrt{\phi_s}$ (b). The solid line is our model, namely (2.33). The symbols are data from previous work. Specifically, empty squares are computations by Ng & Wang (2010), filled squares are computations by Ybert *et al.* (2007) and filled circles are experimental results by Lee *et al.* (2008).

The quantitative agreement between our model and previous numerical work is remarkable. The square root dependence on ϕ_s, evident in figure 2(b) is indeed reproduced by our model. For the coefficient A in (1.1), here we predict $A = 3\sqrt{\pi}/16 \approx 0.332$. In their numerical simulations, Ybert *et al.* (2007) fit (1.1) to their results and obtain $A = 0.325$, whereas Ng & Wang (2010) fit to $A = 0.34$, which are both within about 2 % of our prediction.

For the second coefficient in (1.1), we showed above that a term independent of ϕ_s is indeed the next-order term in the asymptotic expansion, and we obtained $B = 3\ln(1+\sqrt{2})/2\pi \approx 0.421$. Ybert *et al.* (2007) fit $B = 0.44$, which is less than 5 % larger, while Ng & Wang (2010) obtain $B = 0.468$, a value about 10 % above our result.

Evaluating the slip lengths at the same surface fraction, ϕ_s, as in Ng & Wang (2010) and Ybert *et al.* (2007), we find that the error between our simple model, (2.33), and

the numerics from Ng & Wang (2010) is about 1.8 %, while the error between our model and the computations of Ybert *et al.* (2007) is about 3.9 %.

Our geometry implies that $\phi_s \leqslant \pi/4$, but the asymptotic estimate (2.33) loses validity at lower values, as seen in the right-hand side of figure 2(*a*), and as illustrated by its prediction of no-slip ($\lambda = 0$) at $\phi_s = \pi^3/[8\ln(1 + \sqrt{2})]^2 \approx 62$ %.

Regarding the comparison with the experiments of Lee *et al.* (2008), we see that our model (and past computations) are able to predict the correct order of magnitude of the slip length, but do not capture the exact dependence on the surface friction, which appears to be weaker than inverse square root (see figure 2*b*). This disagreement is likely due to the difference in flow field. Lee *et al.* (2008) measure the friction by using a cone-and-plate rheometer with rotation axis perpendicular to the surface plane. As a result, the flow in their device has circular streamlines, and is not always aligned with the lattice periodicity. As a difference, in this study, as well as in Ybert *et al.* (2007) and Ng & Wang (2010), the flow considered is a planar shear flow aligned with the lattice period.

4. Conclusion

In this study, we considered theoretically shear flow past fakir-like superhydrophobic surfaces composed of circular posts located on a doubly periodic rectangular lattice. Using a superposition of point forces with suitably spatially dependent strength, we obtained the total flow as an infinite series of linear equations. In the asymptotic limit of small surface coverage by the posts, the series can be interpreted as Riemann sums, which allowed us to derive analytically the effective surface-slip length in the form of (1.1). In the case of a square lattice, our results were found to be in excellent quantitative agreement with previous numerical computations. Future work will focus on embedding such low-friction-fakir surface on a curved substrate (for example, a sphere), and attempting to predict its mobility coefficient in a viscous fluid.

REFERENCES

Bico, J., Marzolin, C. & Quéré, D. 1999 Pearl drops. *Europhys. Lett.* **47**, 220–226.

Bocquet, L. & Barrat, J.-L. 2007 Flow boundary conditions: from nano- to micro-scales. *Soft Matter* **3**, 685–693.

Choi, C. H. & Kim, C. J. 2006 Large slip of aqueous liquid flow over a nanoengineered superhydrophobic surface. *Phys. Rev. Lett.* **96**, 066001.

Choi, C. H., Ulmanella, U., Kim, J., Ho, C. M. & Kim, C. J. 2006 Effective slip and friction reduction in nanograted superhydrophobic microchannels. *Phys. Fluids* **18**, 087105.

Cottin-Bizonne, C., Barentin, C., Charlaix, E., Bocquet, L. & Barrat, J. L. 2004 Dynamics of simple liquids at heterogeneous surfaces: molecular-dynamics simulations and hydrodynamic description. *Eur. Phys. J.* E **15**, 427–438.

Davies, J., Maynes, D., Webb, B. W. & Woolford, B. 2006 Laminar flow in a microchannel with superhydrophobic walls exhibiting transverse ribs. *Phys. Fluids* **18**, 087110.

Davis, A. M. J. & Lauga, E. 2009 The friction of a mesh-like super-hydrophobic surface. *Phys. Fluids* **21**, 113101.

FENG, L., LI, S. H., LI, Y. S., LI, H. J., ZHANG, L. J., ZHAI, J., SONG, Y. L., LIU, B. Q., JIANG, L. & ZHU, D. B. 2002 Super-hydrophobic surfaces: from natural to artificial. *Adv. Mater.* **14**, 1857–1860.

DE GENNES F. BROCHARD-WYART, P.-G. & QUÉRÉ, D. 2004 *Capillarity and Wetting Phenomena: Drops, Bubbles, Pearls, Waves*. Springer.

GOGTE, S., VOROBIEFF, P., TRUESDELL, R., MAMMOLI, A., VAN SWOL, F., SHAH, P. & BRINKER, C. J. 2005 Effective slip on textured superhydrophobic surfaces. *Phys. Fluids* **17**, 051701.

HAPPEL, J. & BRENNER, H. 1965 *Low Reynolds Number Hydrodynamics*. Prentice Hall.

HASIMOTO, H. 1959 On the periodic fundamental solutions of the Stokes equations and their application to viscous flow past a cubic array of spheres. *J. Fluid Mech.* **5**, 317–328.

JOSEPH, P., COTTIN-BIZONNE, C., BENOIT, J. M., YBERT, C., JOURNET, C., TABELING, P. & BOCQUET, L. 2006 Slippage of water past superhydrophobic carbon nanotube forests in microchannels. *Phys. Rev. Lett.* **97**, 156104.

LAUGA, E., BRENNER, M. P. & STONE, H. A. 2007 Microfluidics: the no-slip boundary condition. In *Handbook of Experimental Fluid Dynamics* (ed. A. Yarin, C. Tropea & J. F. Foss), Chap. 19, pp. 1219–1240. Springer.

LAUGA, E. & STONE, H. A. 2003 Effective slip in pressure-driven Stokes flow. *J. Fluid Mech.* **489**, 55–77.

LEE, C., CHOI, C. H. & KIM, C. J. 2008 Structured surfaces for a giant liquid slip. *Phys. Rev. Lett.* **101**, 064501.

MAYNES, D., JEFFS, K., WOOLFORD, B. & WEBB, B. W. 2007 Laminar flow in a microchannel with hydrophobic surface patterned microribs oriented parallel to the flow direction. *Phys. Fluids* **19**, 093603.

NETO, C., EVANS, D. R., BONACCURSO, E., BUTT, H.-J. & CRAIG, V. S. J. 2005 Boundary slip in Newtonian liquids: a review of experimental studies. *Rep. Prog. Phys.* **68**, 2859–2897.

NG, C.-O. & WANG, C. Y. 2009 Stokes shear flow over a grating: implications for superhydrophobic slip. *Phys. Fluids* **21**, 013602.

NG, C.-O. & WANG, C. Y. 2010 Apparent slip arising from Stokes shear flow over a bidimensional patterned surface. *Microfluid Nanofluid* **8**, 361–371.

ONDA, T., SHIBUICHI, S., SATOH, N. & TSUJII, K. 1996 Super-water-repellent fractal surfaces. *Langmuir* **12**, 2125–2127.

OU, J., PEROT, B. & ROTHSTEIN, J. P. 2004 Laminar drag reduction in microchannels using ultrahydrophobic surfaces. *Phys. Fluids* **16**, 4635–4643.

OU, J. & ROTHSTEIN, J. P. 2005 Drag reduction and μ-PIV measurements of the flow past ultrahydrophobic surfaces. *Phys. Fluids* **17**, 103606.

QUÉRÉ, D. 2008 Wetting and roughness. *Annu. Rev. Fluid Mech.* **38**, 71–99.

ROACH, P., SHIRTCLIFFE, N. J. & NEWTON, M. I. 2008 Progress in superhydrophobic surface development. *Soft Matter* **4**, 224–240.

ROTHSTEIN, J. P. 2010 Slip on superhydrophobic surfaces. *Annu. Rev. Fluid Mech.* **42**, 89–109.

TEO, C. J. & KHOO, B. C. 2009 Analysis of Stokes flow in microchannels with superhydrophobic surfaces containing a periodic array of micro-grooves. *Microfluid Nanofluid* **7**, 353–382.

TRUESDELL, R., MAMMOLI, A., VOROBIEFF, P., VAN SWOL, F. & BRINKER, C. J. 2006 Drag reduction on a patterned superhydrophobic surface. *Phys. Rev. Lett.* **97**, 044504.

TSAI, P. C., PETERS, A. M., PIRAT, C., WESSLING, M., LAMMERTINK, R. G. H. & LOHSE, D. 2009 Quantifying effective slip length over micropatterned hydrophobic surfaces. *Phys. Fluids* **21**, 112002.

YBERT, C., BARENTIN, C., COTTIN-BIZONNE, C., JOSEPH, P. & BOCQUET, L. 2007 Achieving large slip with superhydrophobic surfaces: scaling laws for generic geometries. *Phys. Fluids* **19**, 123601.